



Preparation of Pd–MgO model catalysts by deposition of Pd from aqueous precursor solutions onto Ag(0 0 1)-supported MgO(0 0 1) thin films



Franziska Ringleb, Martin Sterrer*, Hans-Joachim Freund

Department of Chemical Physics, Fritz-Haber-Institut der Max-Planck-Gesellschaft, Faradayweg 4-6, D-14195 Berlin, Germany

ARTICLE INFO

Article history:

Received 3 April 2013

Received in revised form 22 May 2013

Accepted 24 May 2013

Available online 2 June 2013

Keywords:

Catalyst preparation

Model catalyst

Surface science

Palladium

Magnesium oxide

Spectroscopy

CO oxidation

ABSTRACT

The preparation of Pd–MgO model catalysts via liquid-phase deposition of Pd from aqueous Pd precursor solutions was studied. Thin, single-crystalline MgO(0 0 1) films grown on a Ag(0 0 1) substrate were used as support and allowed surface science techniques such as Auger electron spectroscopy, X-ray photoelectron spectroscopy, scanning tunneling microscopy, and temperature programmed desorption to be applied for characterization. Thin MgO(0 0 1) films were unstable and rapidly dissolved in acidic and neutral environments, but remained stable in thickness in alkaline solutions after an initial dissolution of a few layers of MgO. Pd was deposited by exposure of the thin film MgO substrate to alkaline (pH 12) precursor solutions containing Pd-hydroxide complexes. Scanning tunneling microscopy images taken from ultrathin MgO films revealed the formation of Pd particles 3 nm in diameter after thermal decomposition of the precursor at 600 K, as well as roughening of the MgO substrate, including the formation of etch pits, which leads to partial exposure of the Ag substrate. For Pd deposited on thick MgO films, the formation of Pd nanoparticles by thermal decomposition of the adsorbed Pd-hydroxide precursor was followed by X-ray photoelectron spectroscopy. Pd–MgO model catalysts with similar Pd coverage prepared either by liquid-phase deposition or physical vapor deposition in UHV exhibited similar properties, as revealed by their comparable behavior in CO adsorption and CO oxidation.

© 2013 Elsevier B.V. All rights reserved.

1. Introduction

MgO(0 0 1) is, because of its simple geometric and electronic structure, a widely used model support for investigations aiming at elucidating the properties of supported metal particles, in particular, for studies of supported Pd nanoparticles. For example, nucleation and growth of Pd [1–3], its cluster-size dependent CO oxidation activity [4], or the oxidation and restructuring of Pd particles in oxygen environment [5,6] have been investigated using bulk MgO(0 0 1) single-crystals as support. Furthermore, thin MgO(0 0 1) films grown on either Ag(0 0 1) or Mo(0 0 1) supports have been utilized to investigate the nucleation of single Pd atoms [7,8], the reactivity of size-selected Pd clusters [9,10], or the electronic properties of Pd on MgO(0 0 1) [11,12]. The Pd–MgO system has also been intensively studied computationally, including topics such as the fundamental interaction of Pd atoms with the MgO surface and its point defects [13,14], the diffusion of small Pd clusters [15,16],

the morphology of larger Pd particles [17,18], or the oxidation of small Pd clusters [19]. In addition, the fact that Pd particles of well-defined morphology can be prepared on MgO powders provided the basis for detailed investigations into chemisorption properties and reactivity, for example, in CO adsorption, CO hydrogenation, or methanol decomposition [20–23].

From a more applied catalysis point of view, MgO is an interesting material because of its basic properties. It has been reported that the selectivity in the CO hydrogenation reaction over supported Pd catalysts is strongly directed toward oxygenated products when basic oxides such as MgO are used as support itself or as a promoter in Pd catalysts supported by other oxides [24–26], which has been related with the stabilization of formate-type intermediates at the Pd–MgO boundary [21,22]. Another test reaction, where Pd–MgO catalysts give promising results, is phenol hydrogenation [27–29]. It has been shown that both, the Pd dispersion and the long term activity are higher over Pd–MgO compared to Pd–Al₂O₃. The observed differences were explained by the stronger interaction of Pd with MgO and the suppression of coke formation over the basic MgO [28]. The basic properties of MgO have also been suggested to be the origin for the observation of electron-rich Pd particles on

* Corresponding author. Tel.: +49 30 8413 4132.

E-mail address: sterrer@fhi-berlin.mpg.de (M. Sterrer).

this support, a conclusion that has been deduced from reduced Pd binding energies [29] and from the specific stretching frequencies of CO on Pd–MgO catalysts [23,30].

From a practical point of view, the main drawback of MgO is its rather low thermal stability, which limits its use as a support material in heterogeneous catalysis. Although MgO powders with high specific surface area can be prepared, this material strongly sinters following deposition of Pd by wet preparation routes such as impregnation or deposition-precipitation [31]. The reason for the sintering may be found in the instability of MgO in humid and aqueous environment. In particular, in acidic solutions, which are most frequently applied in Pd catalyst preparation by impregnation, dissolution is a more serious problem for ionic oxides such as MgO than for the more covalent oxides such as Al₂O₃ and SiO₂.

The reactivity of MgO toward water and the restructuring and dissolution in aqueous environments represent a challenge for studies aiming at bridging the surface science model approach to catalysis, which utilizes morphologically well-defined samples and ultrahigh vacuum (UHV) methodologies, to studies of dispersed catalysts under realistic environmental conditions. In an attempt to elucidate the influence of surface hydroxyls on the interaction of metals with MgO surfaces, our group has recently investigated the controlled hydroxylation of model MgO(001) thin film surfaces and the nucleation and sintering of gold on hydroxylated MgO [32–34]. In the present work, we take a step further toward realistic conditions and apply a surface science approach to catalyst preparation, using single-crystalline oxide thin films as supports [35,36], to study the preparation of an MgO-supported Pd model catalyst by applying wet-chemical preparation routes. In this study, the stability of Ag(001)-supported MgO(001) thin films in various aqueous environments has first been explored in order to find appropriate conditions for Pd deposition. Next, the thermal decomposition of adsorbed Pd precursor complexes into Pd nanoparticles was studied with X-ray photoelectron spectroscopy (XPS) and scanning tunneling microscopy (STM) for Pd deposited on ultrathin (5 monolayers, ML) and thick (60 ML) MgO films. Finally, CO chemisorption and CO oxidation as probed with temperature programmed desorption (TPD) allowed to compare the properties of Pd–MgO model catalysts prepared by Pd deposition from aqueous precursor solution (liquid phase deposition, LPD) with those of a Pd–MgO sample prepared exclusively in UHV via physical vapor deposition (PVD) of Pd.

2. Experimental

Two separate ultra-high vacuum (UHV) set-ups were used in the present study for preparation and characterization of the samples. Both set-ups are equipped with standard tools for single-crystal sample cleaning and thin oxide film growth. One of the set-ups houses a 4-grid LEED (low energy electron diffraction) optics (Specs) with the option to perform Auger electron spectroscopy (AES), and a differentially pumped quadrupole mass spectrometer (Pfeiffer) for thermal desorption spectroscopy (TDS), while the other set-up is equipped with a hemispherical electron analyzer (Specs Phoibos 150) and a dual anode (Al/Mg) X-ray gun (Specs) for X-ray photoelectron spectroscopy (XPS). Both set-ups have a transfer chamber/load lock attached allowing fast sample transfer between the chambers. In addition to the UHV set-ups, a Wandel-type electrochemical scanning tunneling microscope [37] operated in ambient air was employed for STM investigations.

The Ag(001) substrate used in this study, which was mounted on a modified Omicron molybdenum sample plate, had a diameter of 10 mm and a thickness of 6 mm. The sample could be heated by electron beam heating using a filament attached to the back-side of the plate. A constant positive bias was applied to the sample

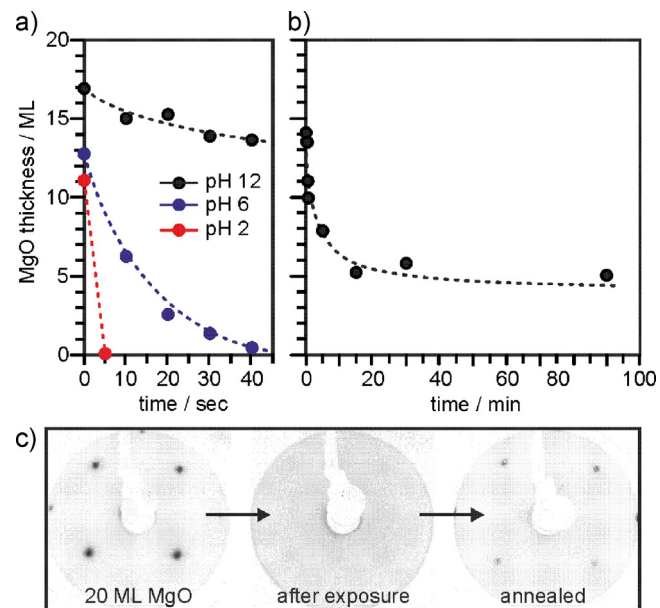


Fig. 1. (a) Dissolution of MgO(001)/Ag(001) films (initial thicknesses corresponding to the values at time = 0 s) in various environments plotted as MgO film thickness vs. time of exposure to solutions; black: 0.01 M NaOH solution (pH 12), blue: Millipore water (pH 6), red: 0.01 M HCl solution (pH 2). (b) Dissolution of MgO(001)/Ag(001) in 0.01 M NaOH. (c) LEED pattern ($E = 70$ eV) of a pristine 20 ML MgO(001)/Ag(001) film (left). No diffraction pattern is obtained from a MgO(001)/Ag(001) film exposed to alkaline solutions (middle). A faint (1×1) LEED pattern is restored after subsequent annealing at 710 K (right). (For interpretation of the references to color in this figure legend, the reader is referred to the web version of the article.)

during heating, while the filament current was controlled with a PID controller. The sample temperature was determined with a type-K thermocouple attached to the sample.

The Ag(001) surface was cleaned by repeated cycles of Ar⁺ sputtering (1×10^{-5} mbar Ar, ~ 6 μ A) at room temperature and subsequent annealing at 700 K in UHV until a sharp (1×1) LEED pattern was obtained and no surface contaminations were detected by AES or XPS. Ag(001)-supported MgO(001) thin films were prepared in the UHV chamber by reactive deposition of Mg from an electron beam evaporator (Omicron EFM 3) in an O₂ background of 1×10^{-6} mbar and with the Ag(001) substrate held at 570 K during deposition. The Mg flux was calibrated with a quartz-microbalance and was adjusted to yield an MgO growth rate of one monolayer (ML)/min. After preparation, the MgO(001)/Ag(001) samples were annealed for 5 min at 700 K in UHV. Surface crystallinity and cleanliness of the MgO(001) films was checked with LEED (see Fig. 1c) and AES/XPS.

For MgO dissolution studies, freshly prepared MgO(001)/Ag(001) samples were transferred out of the UHV chamber into ambient laboratory atmosphere via a transfer chamber/load lock. The contact time to laboratory atmosphere before exposure to the solutions was kept at a minimum and was two minutes at most. The single crystal surface was placed above the solution surface in a hanging meniscus configuration to avoid exposure of the uncovered side planes of the Ag(001) crystal. Millipore water (pH 6), 0.01 M HCl (prepared from 30% HCl, suprapur, Merck), and 0.01 M NaOH (p.a., Merck) were applied in the dissolution studies.

MgO-supported Pd model catalysts were prepared via a wet-chemical route (Pd–MgO LPD), using freshly prepared MgO(001)/Ag(001) thin film samples as supports. After transfer of the thin film samples out of the UHV chamber into laboratory atmosphere, the MgO(001) surface was exposed in a hanging meniscus configuration to alkaline (pH 12) Pd²⁺ precursor solutions. The Pd²⁺

stock solution was prepared by dissolving PdCl_2 (99.9%, Alfa Aesar) in HCl. The final pH and Pd^{2+} concentration of the precursor solution was adjusted by adding water and NaOH. After exposure to Pd^{2+} precursor solutions, the surface was rinsed with 3 ml H_2O in order to remove Na and Cl residues left on the surface from the solutions. All subsequent treatments (thermal decomposition of the precursor, reduction/oxidation treatments, and spectroscopic surface characterization) were carried out in the UHV chamber.

In addition to the samples prepared via the wet-chemical route, Pd–MgO model catalysts prepared exclusively in UHV were investigated in this study (Pd–MgO PVD). For the UHV model catalysts, Pd was evaporated onto clean MgO(001) surfaces in UHV via physical vapor deposition of Pd with the sample surface held at room temperature. The Pd evaporation rate was calibrated with a quartz-microbalance.

3. Results and discussion

3.1. Stability of MgO(001)/Ag(001) films in aqueous solutions

Several previous studies have addressed the morphological changes associated with the attack of water and the dissolution of MgO on both, MgO particles and MgO single-crystal surfaces (e.g. [38–44]). It is well established that proton attack strongly enhances dissolution in acidic media, whereas in alkaline solutions, close to the point of zero charge of MgO ($\text{pzc} \approx 12$), the dissolution rate is small. In line with this, scanning force microscopy studies have identified morphological modifications and the formation of etch pits on the MgO(001) surface upon exposure to acidic and neutral solutions [41,43], while in alkaline solutions a rather flat surface morphology was found to be preserved [45]. A clear view on the surface transformations upon exposure to water was provided by transmission electron microscopy studies using large cubic MgO(001) smoke particles [44,46]. The initial formation of cuts exhibiting [110] truncations is followed at later stages of exposure by the transformation of the MgO cubes into octahedra exposing [111] terminations, in line with the predicted thermodynamic stability of hydrated MgO(111) in humid environment [47].

An important aspect to consider prior to the deposition of Pd from aqueous precursors concerns therefore the stability and rate of dissolution of the MgO thin film substrate in aqueous solutions. The dissolution rates in the experiments reported here have been determined by Auger electron spectroscopy, using O/Ag Auger peak intensity ratios of freshly prepared MgO films with thicknesses between 1 and 20 ML for calibration. This allowed to determine the thickness of MgO films prior and after exposure to solutions. In Fig. 1a, the variation of MgO film thickness as a function of exposure time is displayed for dissolution experiments in acidic (pH 2, 0.01 M HCl), alkaline (pH 12, 0.01 M NaOH) and close to neutral (pH 6, Millipore water) environments, respectively. The data points at $t = 0$ s represent the thickness of the pristine films. The data shown in Fig. 1a is consistent with the expected faster dissolution of MgO in acidic media. In fact, in 0.01 M HCl solution the dissolution is so fast that the film was completely dissolved within the first 5 s of exposure. The dissolution rate is smaller at pH 6; however, even under these conditions a 13 ML thin MgO film was completely dissolved within 40 s of exposure. During the same period, only 3 ML MgO were dissolved from the MgO sample upon exposure to alkaline (pH 12) solutions. For the latter, the dissolution behavior was studied for prolonged exposures (up to 90 min, Fig. 1b), the results of which show that the dissolution is initially fast and considerably slows down with time, until a stable surface state is obtained after 20–30 min of exposure. No diffraction pattern is visible in LEED images taken directly after exposure of the initially well-ordered

MgO(001) films to alkaline solutions (Fig. 1c). This indicates that the reaction of the MgO surface with water and the subsequent partial dissolution is accompanied by surface reconstruction, leading to a strongly disordered surface. Subsequent annealing to 710 K is sufficient to restore a faint (1×1) LEED pattern (Fig. 1c). The LEED results, in combination with XPS data (see, for example, the O 1s spectra reported in Fig. 3a), are compatible with the formation of a strongly hydroxylated, or even brucite (Mg(OH)_2)-like surface layer during exposure to alkaline solution. Poorly ordered MgO(001) is again obtained following dehydroxylation or decomposition of Mg(OH)_2 at elevated temperature.

The initial dissolution rates calculated from Fig. 1a are: $4.1 \times 10^{-9} \text{ mol cm}^{-2} \text{ s}^{-1}$ (pH 2), $9.7 \times 10^{-10} \text{ mol cm}^{-2} \text{ s}^{-1}$ (pH 6), and $1.4 \times 10^{-10} \text{ mol cm}^{-2} \text{ s}^{-1}$ (pH 12). These values are in the range of MgO dissolution rates reported previously [38–42]. The deceleration of dissolution during long-term exposure to alkaline solutions is compatible with the formation of a brucite-like surface layer on MgO, which was found to inhibit MgO dissolution [38]. For comparison, reported dissolution rates for brucite at pH 12 are in the range of $10^{-14} \text{ mol cm}^{-2} \text{ s}^{-1}$ [48].

From the results presented above it is clear that any catalyst preparation study with thin MgO films as used in the present study must be carried out with strongly alkaline precursor solutions in order to avoid complete dissolution of the MgO substrate during the precursor adsorption process. The acidic PdCl_2 precursor solution was, therefore, hydrolyzed by adding NaOH, and care was taken to avoid precipitation of Pd(OH)_2 during the hydrolysis step. At pH 12, which was set for all precursor solutions used in this study, the predominant Pd species in solution are Pd(OH)_4^{2-} complexes [49].

3.2. Pd deposition onto thin (nominally 5 ML) MgO films

Initial Pd deposition experiments were carried out with ultra-thin films in order to allow the morphology of the resulting surfaces to be examined with scanning tunneling microscopy (STM). Fig. 2 shows representative STM images obtained from a Pd–MgO/Ag(001) sample prepared by exposure of a 5 ML MgO(001)/Ag(001) thin film to a 0.5 mM Pd^{2+} (pH 12) precursor solution for 5 min, followed by heating to 600 K in UHV. The larger scale image (160 nm × 110 nm, Fig. 2a) displays a rough surface with morphological features in the range of 10 nm in diameter, clearly different from flat MgO(001) films observed in previous STM investigations in UHV [50]. The increased roughness is a consequence of the structural modifications during the initial partial dissolution of the MgO surface upon exposure to the alkaline precursor solution. Although protrusions with different contrast are observed, a distinction between MgO-related features and Pd nanoparticles is not obvious from Fig. 2a. However, on a smaller scale (Fig. 2b, 100 nm × 60 nm), the distinction between support and Pd nanoparticles becomes more evident. Here, the brighter protrusions, which are assigned to Pd nanoparticles, can clearly be differentiated from the rough support. A few darker spots observed in this image are indicative of small holes down to the Ag(001) substrate. Taking tip convolution effects into account, the diameter of the Pd particles can be estimated to be about 3 nm.

In order to obtain chemical information about the processes of Pd nanoparticle formation on the 5 ML MgO(001)/Ag(001) sample, a similar preparation as the one described above was analyzed with XPS. The clean film exhibits an O 1s photoemission peak at 529.5 eV binding energy (BE) that is typical for a thin, supported MgO film (Fig. 3a, black trace) [51]. This signal gets strongly attenuated upon adsorption of the Pd precursor from aqueous solution (Fig. 3a, blue trace). In addition, a shoulder appears at the high BE side of this peak (532 eV), which can be attributed to the presence of hydroxyls. (Note that the Pd 3p emission is in the same BE range as the O 1s emission. Because of the small concentration of Pd on this surface,

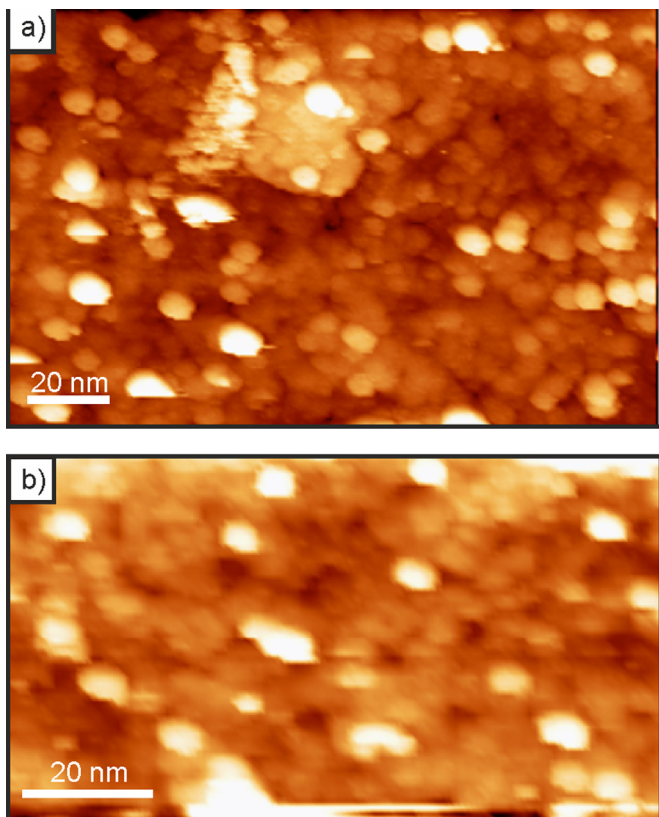


Fig. 2. STM images of a nominally 5 ML thin MgO(001)/Ag(001) film taken in ambient environment after deposition of Pd from aqueous Pd²⁺ precursor (1 mM PdCl₂, pH 12, 5 min) and subsequent thermal annealing at 600 K. (a) 160 nm × 110 nm, (b) 100 nm × 60 nm. Tunneling conditions: $i_t = 100 \text{ pA}$, $U_t = 100 \text{ mV}$.

the shoulder at 532 eV originates almost entirely from hydroxyl species on the MgO surface). The corresponding Pd 3d spectrum displays the typical Pd 3d doublet structure with a separation of 5.3 eV between the Pd_{5/2} and Pd_{3/2} states. The individual components exhibit an additional fine structure, pointing to the presence of at least two chemically different Pd species with Pd 3d_{5/2} BE's of 337.3 and 335.2 eV, respectively (Fig. 3c, blue trace). The high BE component can be assigned to adsorbed precursor complexes of oxidic (hydroxidic) nature, whereas the BE of the second component is compatible with the presence of metallic Pd species. Upon heating to 400 K, partial decomposition of the oxidic precursor into metallic Pd is observed, which is complete after further heating to 600 K. In addition, this heat treatment leads to dehydroxylation of the MgO surface, seen by the disappearance of the shoulder at 532 eV BE in the O 1s region. The integrated area of the Pd 3d signals does not change for samples annealed up to 600 K. This means that no Pd is lost during the first annealing steps. However, the peak intensity of the Pd 3d signal strongly decreases following further heating to 710 K. Note that the O 1s signal of the MgO film is only half as intense after the final annealing step as compared to the initial clean MgO film. This behavior is expected based on the partial dissolution of the MgO film in alkaline solutions. Correspondingly, an increase of the Ag 3d signal intensity is observed (Fig. 3b).

The XPS data provide further support for the assignment of the bright protrusions observed in the STM image (Fig. 2b) to metallic Pd nanoparticles. However, these results also indicate that there is a non-negligible interaction of Pd with the Ag(001) support: The strong diminishment of the Pd 3d signal upon annealing to 710 K likely results from diffusion of Pd into the Ag bulk through holes in the MgO film, which were created during exposure to the precursor solution. Likewise, the presence of metallic Pd on the non-annealed

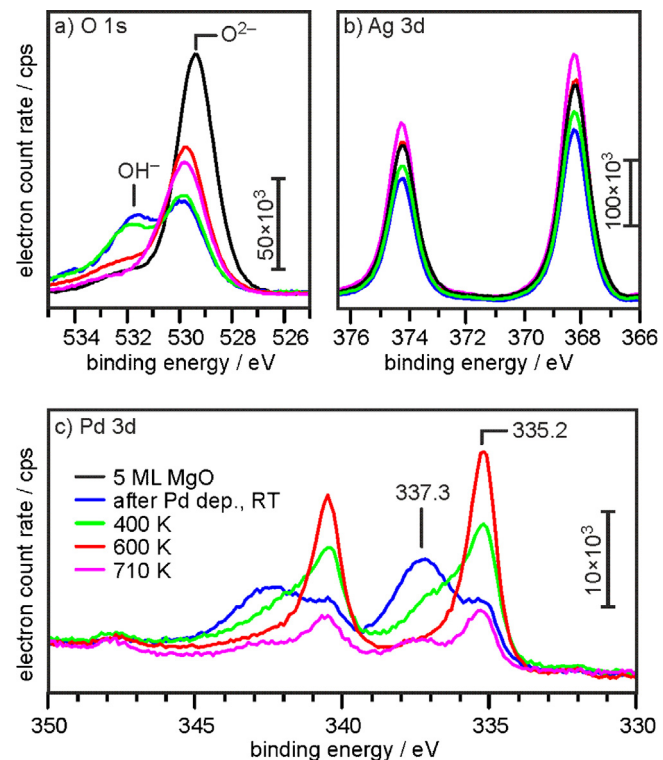


Fig. 3. XP spectra of the O 1s (a), Ag 3d (b) and Pd 3d (c) regions from 5 ML MgO(001)/Ag(001) (black traces), after exposure to aqueous Pd precursor (0.5 mM PdCl₂, pH 12, 5 min) (blue), and after subsequent thermal annealing in UHV at 400 K (green), 600 K (red) and 710 K (magenta). (For interpretation of the references to color in this figure legend, the reader is referred to the web version of the article.)

sample can be ascribed to the direct adsorption and decomposition of Pd precursor complexes on partially exposed Ag(001) support.

3.3. Pd deposition onto thick (nominally 60 ML) MgO films

In order to avoid any contribution from the Ag(001) substrate during the precursor deposition and decomposition stages, the following experiments were performed with nominally 60 ML thick MgO films. Because STM cannot be applied to MgO films of this thickness, the Pd coverage (loading) of Pd–MgO model catalysts, which can be used to estimate the Pd particle size, was determined by quantitative comparison of XPS Pd 3d peak areas from samples obtained by liquid phase deposition (LPD) of Pd, and those prepared by evaporation of known amounts of Pd by physical vapor deposition (PVD) in UHV. Fig. 4a displays the Pd 3d photoemission spectra of samples prepared in the latter way for increasing amounts of Pd evaporated at room temperature (Pd coverage, $\theta(\text{Pd}) = 0.07 \text{ ML}$ (i), 0.18 ML (ii), 0.36 ML (iii), 1.1 ML (iv); 1 ML Pd corresponds to a closed-packed hexagonal layer of Pd atoms, that is $1.5 \times 10^{15} \text{ atoms/cm}^2$). For comparison, the Pd 3d spectra taken directly after 5 min exposure of MgO(001)/Ag(001) thin films to precursor solutions of 0.05 mM (i), 0.5 mM (ii), 1 mM (iii), and 2.5 mM (iv) Pd²⁺, respectively, are shown in Fig. 4b. The plot in Fig. 4c reveals an almost perfect linear correlation between the resulting surface Pd coverage and the Pd²⁺ concentration in the precursor solution. The Pd coverages of the individual samples are summarized in Table 1. In addition, Table 1 provides the corresponding Pd loading in weight-%, calculated with the assumption that the surface area of a typical Pd–MgO powder catalyst is 40 m²/g [29,31].

The determination of the absolute coverage allows also to draw conclusions about the expected Pd particle size.

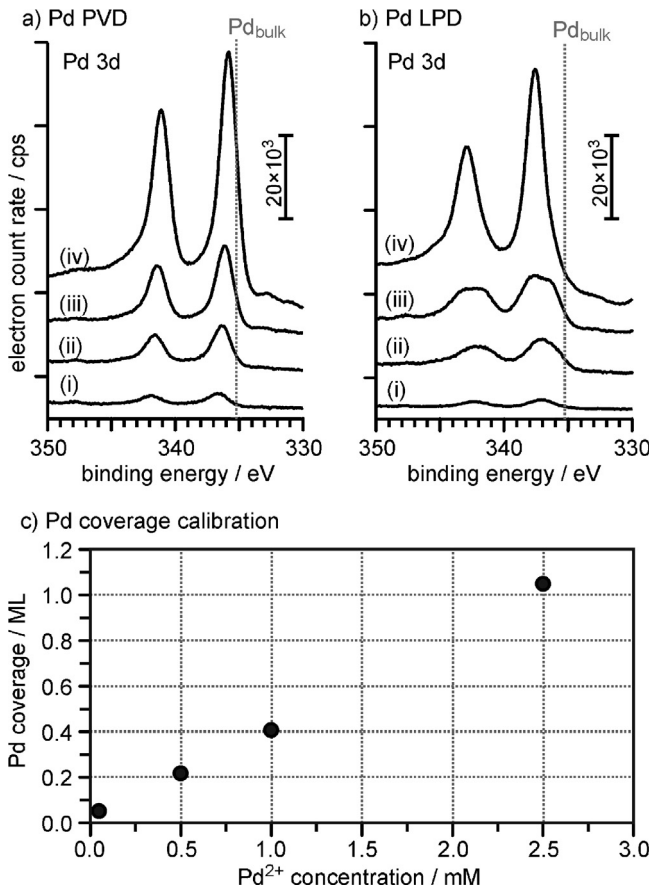


Fig. 4. (a) Pd 3d photoemission spectra from Pd-MgO(001)/Ag(001) samples prepared by physical vapor deposition (PVD); nominal Pd coverage: (i) 0.07 ML, (ii) 0.18 ML, (iii) 0.36 ML, (iv) 1.1 ML. (b) Pd 3d photoemission spectra from Pd-MgO(001)/Ag(001) samples prepared by exposure of the MgO substrate to Pd²⁺ precursor solution (PdCl₂, pH 12, exposure time: 5 min) with various Pd²⁺ concentration; (i) 0.05 mM, (ii) 0.5 mM, (iii) 1 mM, (iv) 2.5 mM. The XP spectra were taken at room temperature directly after deposition and without further annealing. The binding energy of bulk Pd (335.2 eV) is indicated. (c) Relationship between Pd²⁺ concentration in the precursor solution and nominal Pd surface coverage in monolayers.

Although the coverage-dependent Pd cluster size distributions for Pd-MgO(001)/Ag(001) model catalysts have not been determined in UHV, reference to studies on Pd-alumina/NiAl(110) [52] and Pd-Fe₃O₄(111)/Pt(111) [53] from our group as well as on Pd-MgO(001)/Mo(001) from Goodman's group [11] suggests that particle diameters in the range of 1 nm for the samples with the smallest coverage (from 0.05 mM Pd²⁺ precursor solution, $\theta(\text{Pd}) = 0.05 \text{ ML}$), 3 nm for medium Pd coverage (from 1 mM Pd²⁺ precursor solution, $\theta(\text{Pd}) = 0.4 \text{ ML}$), and up to 5 nm for the sample with the largest coverage (from 2.5 mM Pd²⁺ precursor solution, $\theta(\text{Pd}) = 1 \text{ ML}$) are to be expected. The comparison of the Pd-MgO

Table 1

Nominal Pd coverage and calculated Pd loading of Pd-MgO model catalysts obtained by exposure of 60 ML/MgO(001)/Ag(001) to Pd²⁺ precursor solution (pH 12, 5 min exposure time, different Pd²⁺ concentration).

LPD sample (Fig. 4b)	Pd concentration (mM)	Nominal Pd coverage ^a ML	Pd loading ^b (wt.%)
i	0.05	0.05	0.5
ii	0.5	0.22	2.3
iii	1.0	0.41	4.3
iv	2.5	1.05	11.0

^a One ML corresponds to 1.5×10^{15} Pd atoms/cm².

^b Refers to an MgO powder with a specific surface area of 40 m²/g.

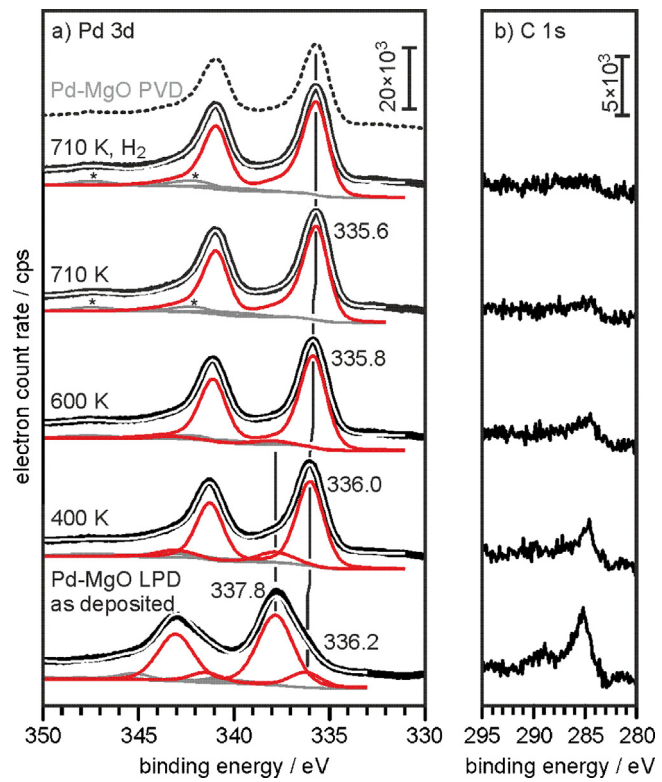


Fig. 5. Pd 3d (a) and C 1s (b) photoemission spectra from a Pd-MgO(0.01)/Ag(0.01) sample prepared by exposure of 60 ML MgO(0.01)/Ag(0.01) to 1 mM Pd²⁺ precursor solution (PdCl₂, pH 12, exposure time: 5 min) taken directly after deposition (bottom, "as deposited"), after subsequent annealing steps in UHV, and after final H₂ reduction (1×10^{-6} mbar, 5 min) at 710 K (top). Bold black lines: experimental spectra; white lines: results of fits; red lines: individual Pd 3d fit components; gray lines: background and contributions due to interband (in oxidic Pd) and Plasmon (in metallic Pd) excitations. The positions of the loss peaks due to Plasmon excitation are marked by stars. For comparison, the Pd 3d XP spectrum of an annealed Pd-MgO PVD sample (nominal Pd coverage: 0.36 ML) is displayed in (a) as dashed line.

LPD samples with UHV-based, oxide-supported Pd model catalyst samples is justified based on the CO chemisorption data presented further below (Section 3.4).

The decomposition of the adsorbed precursor has been studied with XPS for a sample that was prepared by exposure of 60 ML MgO(001)/Ag(001) for 5 min to a 1 mM Pd²⁺ precursor solution, corresponding to a deposited amount of 0.4 ML Pd. Fig. 5a provides Pd 3d photoemission spectra together with results of spectral fitting for the raw catalyst (bottom trace, "as deposited"), and for the same sample following several heating steps. The spectrum of the raw catalyst can be decomposed into two Pd 3d doublets with Pd 3d_{5/2} BE's of 337.8 and 336.2 eV, respectively. Upon heating to 400 K, the high BE component converts almost completely into a Pd species exhibiting a BE of 336.0 eV. Further heating to 600 and 710 K leads to a shift of the main Pd 3d component to 335.8 eV, and finally to 335.6 eV. By comparison of Fig. 5a with Fig. 3c, where a similar decomposition sequence has been employed for Pd deposited on the 5 ML thin MgO film, the absence of the Pd 3d_{5/2} component at 335.2 eV in any of the photoemission spectra taken from the thick film sample is evident. This observation confirms the previous assumption about the active role of Ag in the decomposition of the Pd precursor on the 5 ML thin MgO films (Section 3.2).

The Pd 3d photoemission data recorded at the various stages of Pd precursor decomposition on the thick MgO film sample are qualitatively similar to those reported in our previous study of Pd deposition from alkaline precursor solution onto Fe₃O₄(111) [36]. In agreement with this study and with reported binding energies

of hydroxidic and oxidic Pd species [54–57], Pd-hydroxide precursor complexes adsorb on the MgO surface during exposure to the alkaline Pd^{2+} precursor solution, giving rise to the Pd species with a Pd 3d_{5/2} BE of 337.8 eV. Because the MgO surface is expected to be essentially uncharged at the employed pH, the initial interaction of the precursor with the support surface can be described as hydrolytic interaction of $\text{Pd}(\text{OH})_4^{2-}$ complexes present with surface hydroxyls. The adsorbed Pd-hydroxide precursor complexes easily decompose at a slightly elevated temperature (400 K) into partially oxidized Pd particles exhibiting a Pd 3d_{5/2} BE of 336.0 eV. A shift to 335.6 eV after a thermal treatment at 710 K is indicative for further decomposition, resulting in metallic Pd nanoparticles. It is noted that most of the carbon contamination resulting from exposure of the sample to air and precursor solution is efficiently eliminated from the Pd–MgO model catalyst surface at this stage of activation (Fig. 5b).

The presence of metallic Pd nanoparticles after thermal treatment at 710 K is corroborated by the simultaneous appearance of weak satellite peaks at 342 and 347 eV, which are due to energy losses resulting from Plasmon excitation in metallic Pd systems [58], as well as by the fact that the XP spectrum remains essentially unchanged following a subsequent reductive treatment in H_2 atmosphere (Fig. 5a, top). Furthermore, the similarity between the Pd 3d XP spectra from the annealed Pd–MgO LPD sample and annealed Pd–MgO PVD exhibiting a comparable Pd coverage (dashed line in Fig. 5a) shows that these dissimilar preparation procedures yield supported Pd nanoparticles with identical electronic properties.

The Pd 3d_{5/2} BE of 335.6 eV recorded for metallic Pd nanoparticles on 60 ML MgO(001)/Ag(001) is 0.4 eV higher than that of bulk-like metallic Pd systems (335.2 eV), and considerably higher than the 334.4 eV, recorded by Claus et al. for a Pd–MgO powder sample [29]. Because the MgO films employed in the present study are relatively thick (nominally 60 ML), charging effects could potentially lead to a shift to higher BE. However, this possibility is excluded based on the similarity of the C 1s BE's on the 60 ML MgO sample and on the 5 ML MgO sample, where charging effects are negligible. Alternatively, the BE shift could arise from (i) reduced final state screening of the core hole created during the photoemission process in the small Pd particles on the insulating support (final state effect), (ii) initial state contributions such as charge transfer between the MgO support and the Pd particles or lattice contraction in small Pd particles, or (iii) some combination of (i) and (ii). Auger parameter analysis is a potential method to discriminate between those effects [59–61]. A preliminary analysis of the Auger parameter involving the Pd 3d core level BE and the Pd L₃M₄₅M₄₅ Auger transition suggests that the Pd particles are essentially neutral. The observed 0.4 eV shift to higher BE is therefore caused by a reduced final state screening in the small Pd particles. This interpretation is corroborated by the fact that the Pd 3d_{5/2} BE approaches 335.2 eV, that is, bulk-like behavior, in samples with higher Pd coverage that contain larger Pd particles. For example, on a sample prepared by exposure of MgO to 2.5 mM Pd^{2+} precursor solution, which results in a coverage of about 1 ML Pd, the Pd 3d_{5/2} BE obtained after a thermal treatment at 710 K is 335.3 eV (data not shown).

3.4. Comparison of Pd–MgO(001)/Ag(001) model catalysts

In order to explore the chemisorption properties of the Pd–MgO model catalysts, and to investigate whether or not the applied preparation procedure affects the surface properties of the activated catalysts, TPD experiments have been performed for both, a catalyst prepared by application of the Pd precursor via the wet route (Pd–MgO LPD, exhibiting a Pd coverage of approximately 0.4 ML Pd), and for a model catalyst with a similar Pd coverage prepared by physical vapor deposition of Pd onto a pristine MgO(001)

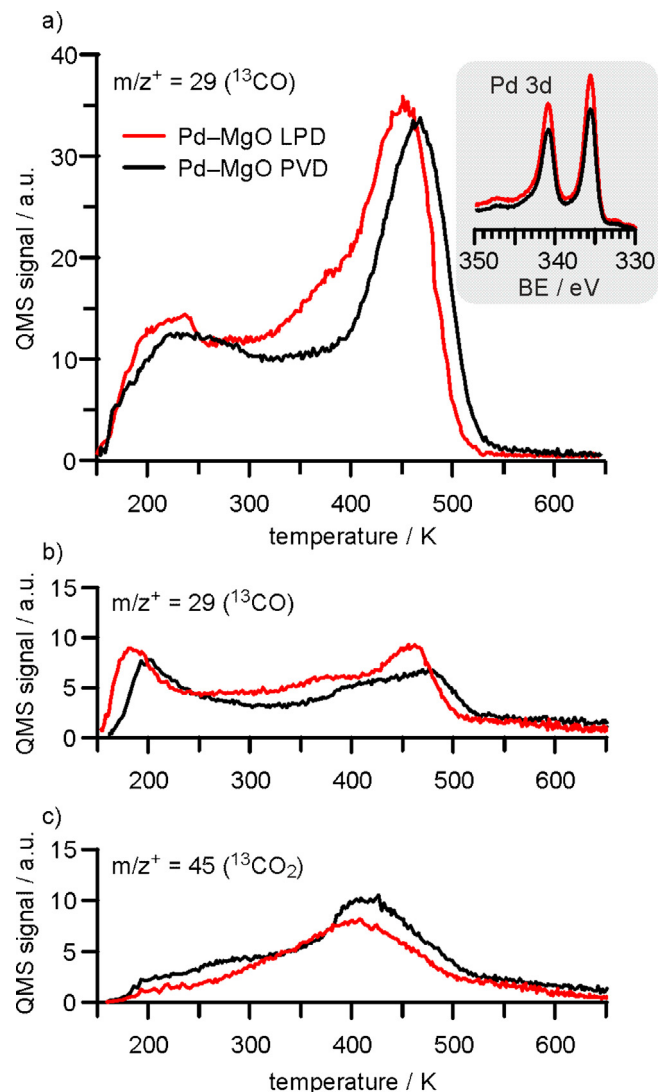


Fig. 6. (a) ^{13}CO TPD traces following adsorption of ^{13}CO at 150 K. (b) ^{13}CO and (c) $^{13}\text{CO}_2$ TPD traces following oxidation of Pd nanoparticles at 400 K and subsequent CO adsorption at 150 K. Red traces: Pd–MgO LPD; black traces: Pd–MgO PVD. The inset in (a) shows the Pd 3d photoemission spectra from the Pd–MgO LPD (red) and Pd–MgO PVD (black) samples, respectively. A constant heating rate of 2 K/s was applied in all TPD experiments. (For interpretation of the references to color in this figure legend, the reader is referred to the web version of the article.)

surface in UHV (Pd–MgO PVD). Prior to the TPD experiments, both samples were subjected to the same activation procedure, which consisted of thermal annealing in UHV at 710 K, followed by an oxidation (O_2)/reduction (H_2) treatment at 600 K. The inset in Fig. 6a provides the Pd 3d photoemission spectra from both samples taken after activation, which shows that the difference in the deposited amount of Pd is small and in a range that is acceptable for direct comparison.

The CO-TPD spectrum from the Pd–MgO PVD sample taken after a saturation ^{13}CO dose at 150 K (black trace in Fig. 6a) is similar to previous CO-TPD data from other oxide-supported Pd model catalysts (e.g. [62,63]). Desorption of CO bound linearly to Pd gives rise to the constant CO desorption rate between 200 and 400 K, whereas the maximum, which is observed here at 465 K, is assigned to desorption of more strongly bound, multiple-coordinated (mainly 3-fold coordinated) CO. The shape of this TPD trace is indicative for the presence of well-faceted Pd nanoparticles on the clean MgO(001) support. In passing to the CO-TPD from the Pd–MgO LPD sample (Fig. 6a, red trace), it can first be noted that the amount of

CO desorbing from this sample is slightly higher than from Pd–MgO PVD, reflecting the small difference in Pd coverage. The good correlation between integral CO desorption and Pd coverage allows to conclude that the mean Pd particle sizes, the fraction of Pd surface atoms, and the particle density are similar on both samples. There are, however, slight differences in the CO-TPD trace of Pd–MgO LPD compared to Pd–MgO PVD that are worth mentioning: the desorption maximum is shifted to lower temperature (450 K), and increased CO desorption is observed between 350 and 400 K. It has to be noted that CO desorption from Pd–Ag alloys vs. pure Pd shows a characteristic deviation with similar features as observed here for Pd–MgO LPD vs. Pd–MgO PVD [67]. The formation of Pd–Ag alloy particles on Pd–MgO LPD can, however, be excluded based on the observation of a large fraction of CO desorbing from multiple-coordinated sites (which is strongly suppressed in Pd–Ag alloys), as well as by the fact that the same Pd 3d BE's are recorded for Pd–MgO LPD and Pd–MgO PVD.

With reference to previous TPD studies (Pd(1 1 1) [64], Pd(1 1 2) [65], and Pd foils [66]), the differences observed between the CO TPD's of Pd–MgO LPD and Pd–MgO PVD can therefore be related to a slightly higher abundance of low-coordinated Pd atoms on the surface of the Pd nanoparticles over Pd–MgO LPD. Similar conclusions have been obtained for Pd–Fe₃O₄(1 1 1) model catalysts [36].

Finally, the activity of the LPD and PVD samples in CO oxidation has been studied. For this purpose, TPD spectra were recorded following saturation doses with O₂ (dosed at 400 K) and ¹³CO (dosed at 150 K). The corresponding ¹³CO and ¹³CO₂ traces are displayed in Fig. 6b and c, respectively. Only small differences are observed in the ¹³CO₂ production form Pd–MgO LPD and Pd–MgO PVD and the maximum ¹³CO₂ desorption occurs at around 400–420 K, in perfect agreement with previous studies [63].

In summary, the quite similar chemisorption and activity results obtained with TPD, together with the observation of similar Pd 3d BE's in XPS, suggests that the morphological and chemical properties of activated MgO-supported Pd model catalyst samples exhibiting comparable Pd coverage are only marginally influenced by the Pd loading techniques used in this study. This observation is explained by the fact that Pd deposition via adsorption of Pd-hydroxide complexes, followed by thermal decomposition in UHV, provides a preparation route which leaves the catalyst surface free of precursor residues (Cl⁻, Na⁺) such that Pd particle growth at elevated temperature is mainly governed by thermal sintering, as in the case of the PVD sample. The origin for the formation of slightly more irregular Pd particles when prepared via the wet route may be found in the modified interfacial properties of the MgO support surface. Both, the increased roughness and the presence of hydroxyl groups after exposure to alkaline solutions contribute to a greater variety of adsorption/nucleation sites on Pd–MgO LPD and, hence, to a modified sintering behavior as compared to Pd–MgO PVD.

4. Conclusions

MgO(0 0 1) thin films grown on a Ag(0 0 1) substrate have been utilized as support in a surface science model study aiming at the investigation of Pd–MgO model catalyst preparation using wet chemical preparation procedures. The applicability of MgO thin films in these studies is limited by MgO dissolution in aqueous solutions, which is fast in acidic and neutral environment, but exhibits an acceptable slow rate in strongly alkaline environment. Exposure of MgO films to a pH 12 Pd²⁺ precursor solution results in the initial adsorption of Pd-hydroxide complexes, the surface concentration of which linearly depends on the Pd²⁺ precursor concentration in solution. On 60 ML MgO films, where any influence from the Ag(0 0 1) substrate to the surface chemistry can be excluded,

thermal decomposition of the adsorbed Pd-hydroxide complexes yields metallic Pd nanoparticles, which exhibit morphological and chemical properties comparable to Pd–MgO model catalysts prepared in UHV. The slightly greater abundance of low-coordinated Pd sites present on model catalysts prepared via the wet-chemical route is explained by the modification of the interfacial properties due to increased surface roughness and the presence of hydroxyl groups.

Acknowledgment

Financial support by the Fonds der Chemischen Industrie, Deutsche Forschungsgemeinschaft through the Cluster of Excellence UNICAT, and the European Research Council (ERC Starting Grant No. 280070) is gratefully acknowledged.

References

- [1] C.R. Henry, C. Chapon, C. Duriez, S. Giorgio, Surf. Sci. 253 (1991) 177–189.
- [2] G. Renaud, R. Lazzari, C. Revenant, A. Barbier, M. Noblet, O. Ulrich, F. Leroy, J. Jupille, Y. Borensztein, C.R. Henry, J.P. Deville, F. Scheurer, J. Mane-Mane, O. Fruchart, Science 300 (2003) 1416–1419.
- [3] G. Haas, A. Menck, H. Brune, J.V. Barth, J.A. Venables, K. Kern, Phys. Rev. B 61 (2000) 11105–11108.
- [4] C. Becker, C.R. Henry, Surf. Sci. 352 (1996) 457–462.
- [5] P. Nolte, A. Stierle, N. Kasper, N.Y. Jin-Phillipp, H. Reichert, A. Rühm, J. Okasinski, H. Dosch, S. Schöder, Phys. Rev. B 77 (2008).
- [6] P. Nolte, A. Stierle, N. Kasper, N.Y. Jin-Phillipp, N. Jeutter, H. Dosch, Nano Lett. 11 (2011) 4697–4700.
- [7] M. Sterrer, T. Risse, L. Giordano, M. Heyde, N. Nilius, H.-P. Rust, G. Pacchioni, H.-J. Freund, Angew. Chem. Int. Ed. 46 (2007) 8703–8706.
- [8] M. Sterrer, T. Risse, U.M. Pozzani, L. Giordano, M. Heyde, H.-P. Rust, G. Pacchioni, H.-J. Freund, Phys. Rev. Lett. 98 (2007) 096107.
- [9] S. Abbet, A. Sanchez, U. Heiz, W.D. Schneider, J. Catal. 198 (2001) 122–127.
- [10] M.A. Roettgen, S. Abbet, K. Judai, J.-M. Antonietti, A.S. Woerz, M. Arenz, C.R. Henry, U. Heiz, J. Am. Chem. Soc. 129 (2007) 9635–9639.
- [11] C. Xu, W.S. Oh, G. Liu, D.Y. Kim, D.W. Goodman, J. Vac. Sci. Technol. A 15 (1997) 1261–1268.
- [12] Q. Guo, P.J. Moller, J. Phys. Chem. C 114 (2010) 18167–18172.
- [13] V.A. Nasluzov, V.V. Rivanenkov, A.B. Gordienko, K.M. Neyman, U. Birkenheuer, N. Rösch, J. Chem. Phys. 115 (2001) 8157–8171.
- [14] L. Giordano, J. Goniakowski, G. Pacchioni, Phys. Rev. B 64 (2001) 075417.
- [15] L.J. Xu, G. Henkelman, C.T. Campbell, H. Jonsson, Phys. Rev. Lett. 95 (2005) 146103.
- [16] G. Barcaro, A. Fortunelli, F. Nita, R. Ferrando, Phys. Rev. Lett. 95 (2005) 246103.
- [17] G. Barcaro, A. Fortunelli, G. Rossi, F. Nita, R. Ferrando, Phys. Rev. Lett. 98 (2007) 156101.
- [18] G. Rossi, C. Mottet, F. Nita, R. Ferrando, J. Phys. Chem. B 110 (2006) 7436–7442.
- [19] B. Huber, P. Koskinen, H. Häkkinen, M. Moseler, Nat. Mater. 5 (2006) 44–47.
- [20] S. Bertarione, D. Scarano, A. Zecchina, V. Johanek, J. Hoffmann, S. Schauermann, M.M. Frank, J. Libuda, G. Rupprechter, H.-J. Freund, J. Phys. Chem. B 108 (2004) 3603–3613.
- [21] S. Bertarione, D. Scarano, A. Zecchina, V. Johanek, J. Hoffmann, S. Schauermann, J. Libuda, G. Rupprechter, H.-J. Freund, J. Catal. 223 (2004) 64–73.
- [22] H. Borchert, B. Jürgens, V. Zielasek, G. Rupprechter, S. Giorgio, C.R. Henry, M. Bäumer, J. Catal. 247 (2007) 145–154.
- [23] E. Groppo, S. Bertarione, F. Rotunno, G. Agostini, D. Scarano, R. Pellegrini, G. Leofanti, A. Zecchina, C. Lamberti, J. Phys. Chem. C 111 (2007) 7021–7028.
- [24] Y.A. Ryndin, R.F. Hicks, A.T. Bell, Y.I. Yermakov, J. Catal. 70 (1981) 287–297.
- [25] J.M. Driessens, E.K. Poels, J.P. Hindermann, V. Ponec, J. Catal. 82 (1983) 26–34.
- [26] A. Gotti, R. Prins, J. Catal. 175 (1998) 302–311.
- [27] S. Galvagno, A. Donato, G. Neri, R. Pietropaolo, J. Chem. Technol. Biotechnol. 51 (1991) 145–153.
- [28] N. Mahata, V. Vishwanathan, J. Catal. 196 (2000) 262–270.
- [29] P. Claus, H. Berndt, C. Mohr, J. Radnik, E.J. Shin, M.A. Keane, J. Catal. 192 (2000) 88–97.
- [30] M. Kappers, C. Dossi, R. Psaro, S. Recchia, A. Fusi, Catal. Lett. 39 (1996) 183–189.
- [31] H.P. Aytam, V. Akula, K. Janmanchi, S.R.R. Kamaraju, K.R. Panja, K. Gurram, J.W. Niemantsverdriet, J. Phys. Chem. B 106 (2002) 1024–1031.
- [32] E. Carrasco, M.A. Brown, M. Sterrer, H.-J. Freund, K. Kwapien, M. Sierka, J. Sauer, J. Phys. Chem. C 114 (2010) 18207–18214.
- [33] M.A. Brown, E. Carrasco, M. Sterrer, H.-J. Freund, J. Am. Chem. Soc. 132 (2010) 4064–4065.
- [34] M.A. Brown, Y. Fujimori, F. Ringleb, X. Shao, F. Stavale, N. Nilius, M. Sterrer, H.-J. Freund, J. Am. Chem. Soc. 133 (2011) 10668–10676.
- [35] H.F. Wang, H. Ariga, R. Dowler, M. Sterrer, H.-J. Freund, J. Catal. 286 (2012) 1–5.
- [36] H.F. Wang, W.E. Kaden, R. Dowler, M. Sterrer, H.-J. Freund, Phys. Chem. Chem. Phys. 14 (2012) 11525–11533.
- [37] M. Wilms, M. Kruft, G. Bermes, K. Wandelt, Rev. Sci. Instrum. 70 (1999) 3641–3650.

- [38] D.A. Vermilyea, J. Electrochem. Soc. 116 (1969) 1179–1183.
- [39] O. Frühwirth, G.W. Herzog, I. Hollerer, A. Rachetti, Surf. Technol. 24 (1985) 301–317.
- [40] R.L. Segall, R.S.C. Smart, P.S. Turner, J. Chem. Soc. Faraday Trans. 74 (1978) 2907–2912.
- [41] G. Jordan, S.R. Higgins, C.M. Eggleston, Am. Mineral. 84 (1999) 144–151.
- [42] A. Fedorockova, P. Raschman, Chem. Eng. J. 143 (2008) 265–272.
- [43] J.A. Mejias, A.J. Berry, K. Refson, D.G. Fraser, Chem. Phys. Lett. 314 (1999) 558–563.
- [44] R. Hacquart, J. Jupille, J. Cryst. Growth 311 (2009) 4598–4604.
- [45] P. Thissen, V. Thissen, S. Wippermann, Y.J. Chabal, G. Grundmeier, W.G. Schmidt, Surf. Sci. 606 (2012) 902–907.
- [46] R. Hacquart, J. Jupille, Chem. Phys. Lett. 439 (2007) 91–94.
- [47] K. Refson, R.A. Wogelius, D.G. Fraser, M.C. Payne, M.H. Lee, V. Milman, Phys. Rev. B 52 (1995) 10823–10826.
- [48] O.S. Pokrovsky, J. Schott, Geochim. Cosmochim. Acta 68 (2004) 31–45.
- [49] J.J. Cruywagen, R.J. Kriek, J. Coord. Chem. 60 (2007) 439–447.
- [50] S. Schintke, S. Messerli, M. Pivetta, F. Patthey, L. Libioulle, M. Stengel, A. De Vita, W.D. Schneider, Phys. Rev. Lett. 87 (2001) 276801.
- [51] S. Altieri, L.H. Tjeng, F.C. Voogt, A. Hibma, G.A. Sawatzky, Phys. Rev. B 59 (1999) R2517–R2520.
- [52] M. Bäumer, H.-J. Freund, Prog. Surf. Sci. 61 (1999) 127–198.
- [53] T. Schalow, B. Brandt, D.E. Starr, M. Laurin, S.K. Shaikhutdinov, S. Schaueremann, J. Libuda, H.-J. Freund, Phys. Chem. Chem. Phys. 9 (2007) 1347–1361.
- [54] K.S. Kim, A.F. Gossmann, N. Winograd, Anal. Chem. 46 (1974) 197–200.
- [55] C. Furlani, G. Mattogno, V. Sessa, J. Less-Common Met. 102 (1984) 89–96.
- [56] K. Otto, L.P. Haack, J.E. de Vries, Appl. Catal. B Environ. 1 (1992) 1–12.
- [57] T. Pillo, R. Zimmermann, P. Steiner, S. Hüfner, J. Phys. Condens. Matter 9 (1997) 3987–3999.
- [58] F.P. Netzer, M.M. El Gomati, Surf. Sci. 124 (1983) 26–38.
- [59] C.D. Wagner, A. Joshi, J. Electr. Spectrosc. Rel. Phenom. 47 (1988) 283–313.
- [60] G. Hohlneicher, H. Pulm, H.J. Freund, J. Electr. Spectrosc. Rel. Phenom. 37 (1985) 209–224.
- [61] B. Richter, H. Kuhlenbeck, H.J. Freund, P.S. Bagus, Phys. Rev. Lett. 93 (2004) 026805.
- [62] S. Shaikhutdinov, M. Heemeier, J. Hoffmann, I. Meusel, B. Richter, M. Bäumer, H. Kuhlenbeck, J. Libuda, H.-J. Freund, R. Oldman, S.D. Jackson, C. Konvicka, M. Schmid, P. Varga, Surf. Sci. 501 (2002) 270–281.
- [63] X.P. Xu, D.W. Goodman, J. Phys. Chem. 97 (1993) 7711–7718.
- [64] X.C. Guo, J.T. Yates, J. Chem. Phys. 90 (1989) 6761–6766.
- [65] R.D. Ramsier, K.W. Lee, J.T. Yates, Surf. Sci. 322 (1995) 243–255.
- [66] G.M. Bliznakov, M.P. Kiskinova, J. Catal. 61 (1980) 305–309.
- [67] N.A. Khan, A. Uhl, S. Shaikhutdinov, H.-J. Freund, Surf. Sci. 600 (2006) 1849–1853.